Numerical simulation of fusion zone shape of lotus-type porous metals produced by laser welding†

TSUMURA Takuya *, NAKAJIMA Hideo ** and NAKATA Kazuhiro *

KEY WORDS: (Lotus-type porous metal) (Laser welding) (Anisotropy) (Thermal diffusivity) (Laser absorption coefficient)

1. Introduction

Lotus- and Gasar- type porous metals had been developed by Boiko et al. [1, 2] and Nakajima et al. [3-5] and these were expected as innovative engineering materials because the directional pore yields various unique properties [6]. Laser weldability of the lotus-type porous copper [7], iron [8] and magnesium [9] was investigated, and the effect of pore direction on laser fusion zone shape of the magnesium [10-12] and the copper [11,12] by using the results of 3D FEM analysis of temperature distribution during welding were demonstrated. These have pointed out that the relation between direction of the pores and the laser irradiated direction appreciably influence weld formation.

In the present paper, we performed 3D FEM analysis of temperature distribution during laser welding for the lotus-type porous iron and compared the fusion zone shape with those cross sections obtained by experiments [8]. We also estimated the anisotropy of thermal diffusivity inherent in the lotus-type porous metals, and the anisotropy of the laser absorption coefficient caused by the phenomenon of multiple reflections of laser on the wall of pores.

2. Experimental procedure and results

Table 1 shows properties of the lotus-type porous metals used; They are Lotus copper [4-6, 7, 13, 14], Lotus magnesium [6, 9, 15-17], and Lotus iron [8, 18]. These metals exhibited different thermal conductivity along and normal to the directional pores [14]. In order to demonstrate the effect of this characteristic on the welding phenomena, three different combinations of relationships - pore direction, applied heat source direction, and welding direction- were considered as shown in **Fig. 1**.

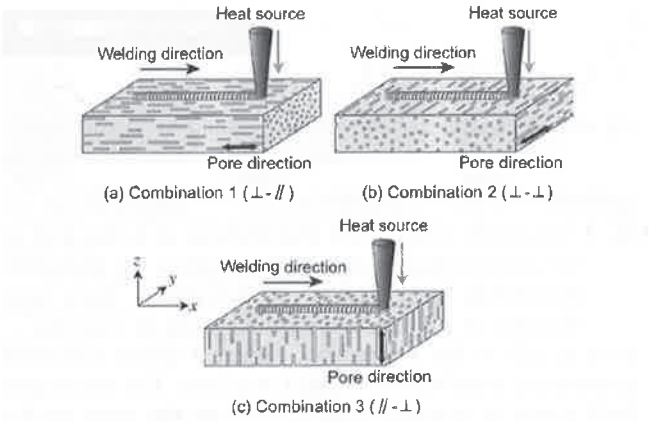

Fig. 1 Schematic views of the lotus-type porous metals showing combinations of pore direction, applied heat source direction, and welding direction.

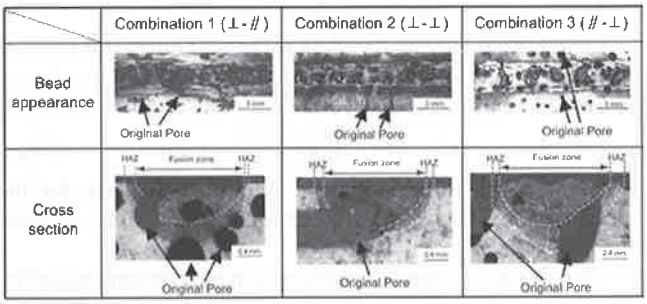

Fig. 2 Bead appearance and cross section of Lotus iron welds; laser power of 1.0 kW, laser spot diameter of 1.0 mm, and welding speed of 1 m·min^{-1} [8].

Laser welding was conducted using an Nd:YAG laser unit. Laser beam irradiated the specimen surface with spot diameter of 0.45 - 1.0 mm at irradiate angles of 10-32° as shown in **Table 1**. Argon with a flow rate of 25-30 l·min^{-1} was used during welding. Cross sections of the welded samples were observed with a digital microscopy.

Figure 2 shows bead appearance and cross section of the Lotus iron [8]. Fusion zone shape and penetration depth of the weld bead has little difference for three combinations.

Table 1 Properties of the lotus-type porous metals and laser irradiate conditions.

	*Absorptivity of base metal** (%)	Porosity (%)	Average pore diameters (μm)	Plate thickness (mm)	Irradiate angle (°)	Number of multiple reflection	Absorption coefficient β	Absorption coefficient β′
Lotus copper	3	30	100	3	10	5	0.03	0.0634
Lotus magnesium	26	35	150	1.8	10	2	0.26	0.3273
Lotus iron	41	17	370	2	32	3	0.41	0.4754

* wavelength: 1000nm at R.T [19]

† Received on 30 September 2010
* JWRI, Osaka University, Ibaraki, Japan
** ISIR, Osaka University, Ibaraki, Japan

Transactions of JWRI is published by Joining and Welding Research Institute, Osaka University, Ibaraki, Osaka 567-0047, Japan

3. Numerical simulation and discussions

3D FEM calculations of temperature distribution of the Lotus iron were performed using ABAQUS with user-defined subroutines. The Lotus iron is modeled as an equivalent orthotropic material. Equivalent density, equivalent specific heat, and thermal conductivity along and normal to the directional pores with temperature dependencies are described by the pore volume content ratio ε and the property of non-porous iron (AISI1006) [20].

Fusion shape of the weld metal is estimated by the cross section of maximum temperature exceeding the melting point at half of the x direction. **Figure 3** shows maximum temperature distributions of the Lotus iron. The absorbable laser power is assumed to 0.522 kW as the most similar results between the experimental fusion depth and the calculated ones for the Combination 2 $(\perp - \perp)$. Fusion zone shape has little difference, and the calculated shapes and the experimental ones were similar.

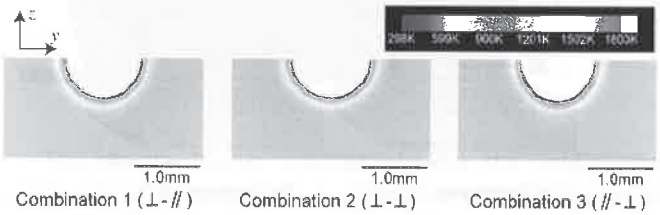

Fig. 3 Maximum temperature distributions of Lotus iron in the cross section at half of the welding (x) direction; absorbable laser power of 0.522 kW, laser spot diameter of 1.0 mm, and welding speed of 1 m·min^{-1}.

The reason is considered as follows; Equivalent thermal diffusivity along and normal to the directional pores are described as follows:

$$\alpha_{eq}^{//} = \alpha_n, \quad \alpha_{eq}^{\perp} = (1+\varepsilon)^{-1}\,\alpha_n \qquad (1).$$

Table 2 shows the equivalent thermal diffusivity for the used metals. The difference between these values is small for the Lotus iron.

Anisotropy of the laser absorption coefficient caused by the phenomenon of multiple reflections of laser on the wall of open pores is also considered; Number of multiple reflections n is described by:

$$n = \mathrm{int}(t \cdot \tan\theta / d) \qquad (2).$$

Here, t is sample thickness, θ is laser irradiated angle, d is average pore diameter. Equivalent heat input along and normal to the directional pores are described as follows:

$$Q_{in}^{\perp} = \beta Q, \quad Q_{in}^{//} = [(1-\varepsilon)\beta + (1-(1-\beta)^n)\varepsilon]Q = \beta' Q \qquad (3).$$

Therefore, laser absorption coefficient β and β' are determined as shown in **Table 1**. There is very little difference between β and β'.

4. Conclusions

The conclusions of this study are summarized as follows.

(1) Fusion zone shape of the weld bead has little difference for three combinations. Calculated shapes and the experimental ones were similar.

(2) The difference between the equivalent thermal diffusivity along and normal to the directional pores is small for the Lotus iron.

(3) The little difference of laser absorption coefficient β and β' for the Lotus iron.

Acknowledgment

This research was supported as part of the entrusted project "development of lightweight high stiffness structural materials and evaluation technology" for the "advanced machining system development project" in the fiscal year 2005 consigned by NEDO. The authors gratefully appreciate this support.

Table 2 Estimated thermal properties of material used at room temperature.

	Base material	Thermal properties of base material (teken form the handbook [21])			Estimated thermal properties of lotus-type porous metals used			
		ρ_n (Kg m^{-3})	$C_{p\,n}$ (J Kg^{-1} K^{-1})	k_n (W m^{-1} K^{-1})	ε (%)	$\alpha^{\perp}_{eq}$ (×10^{-5} m^2 s^{-1})	$\alpha^{//}_{eq}$ (×10^{-5} m^2 s^{-1})	$\alpha^{\perp}_{eq}/\alpha^{//}_{eq}$
Lotus copper	Copper	8880	386	398	30	8.93	11.61	0.740
Lotus magnesium	Magnesium	1737	1020	156	35	6.52	8.80	0.769
Lotus iron	Iron	7850	465	43	17	1.01	1.18	0.854

References

[1] L.V. Boiko *et al.*: Sov. Powder Metal. Met. Ceram., 30 (1991), pp. 78-81.
[2] L.V. Boiko: Mater. Sci., 36 (2000), pp. 506-512.
[3] S.K. Hyun *et al.*: *Proc. Int. Conf. Solid-Solid Phase Transformations '99 (JIMIC-3)*, (1999), pp. 341-344.
[4] H. Nakajima *et al.*: Coloids Surfaces A, 179 (2001), pp. 209-214.
[5] S.K. Hyun *et al.*: Mater. Sci. Eng. A, 299 (2001),pp.241-248.
[6] H. Nakajima: Prog. Mater. Sci., 52 (2007), pp. 1091-1173.
[7] T. Murakami *et al.*: Mater. Sci.Eng.A,357(2003),pp.134-140.
[8] H. Yanagino *et al.*: Mater. Trans., 47 (2006), pp. 2254-2258.
[9] T. Murakami *et al.*: Mater. Sci.Eng.A,456(2007),pp.278-285.
[10] T. Tsumura *et al.*: Mater. Sci. Forum, 502 (2005), pp. 499-504.
[11] T. Tsumura *et al* : Mater. Trans., 47 (2007), pp. 2248-2253.
[12] T. Tsumura *et al.*: Soild State Phenomena, 127 (2007), pp. 307-312.
[13] S.K. Hyun *et al.*: Mater. Sci. Eng. A, 340 (2003), pp. 258-264.
[14] T. Ogushi *et al* : J. Appl. Phys., 95 (2004), pp. 5843-5847.
[15] T. Ikeda *et al.*: J. Jpn. Foundry Eng. Soc. 74 (2002), pp. 812-816 (in Japanese).
[16] T. Ikeda *et al.*: J. Jpn. Inst. Light Met. 54 (2004), pp. 388-393 (in Japanese).
[17] Z.K. Xie *et al.*: Jpn. J. Appl. Phys. 43 (2004), pp. 7315-7319.
[18] M. Tane *et al.*: Acta Mater. 52 (2004), pp. 5195-5201.
[19] E.A. Brandes: *Smithells Metal Reference Book, 6th ed.*, Butterworth London, (1983), p. 17-7.
[20] M.R. Frewin *et al.*: Welding Research Supplement, (1999), pp. 15s-22s.
[21] Japan Society of Thermophysical Properties Ed.: *Thermophysical Properties Handbook*, Yokendo LTD. Tokyo, (1990), p. 23 (in Japanese).